



Synthesis and electrochemical properties of Zn-doped, carbon coated lithium vanadium phosphate cathode materials for lithium-ion batteries

Yuxia Yang, Wenwen Xu, Ruisong Guo^{*}, Lan Liu, Shanshan Wang, Dong Xie, Yizao Wan

Key Laboratory of Advanced Ceramics and Machining Technology, Ministry of Education, Tianjin University, Tianjin 300072, China

HIGHLIGHTS

- Zn-doped $\text{Li}_3\text{V}_2(\text{PO}_4)_3/\text{C}$ were synthesized by an improved sol–gel method.
- Zn doping had an obvious influence on particle size of the prepared powders.
- Zn-doped samples exhibited higher electrical conductivity.
- The cyclability and rate performance were improved significantly by Zn doping.
- Zn-doped cathode showed increased charge-transfer reaction and Li-ion diffusion.

ARTICLE INFO

Article history:

Received 24 March 2014
Received in revised form
26 May 2014
Accepted 1 July 2014
Available online 9 July 2014

Keywords:

Lithium ion battery
Cathode material
Lithium vanadium phosphate
Zn-doping
Electrochemical performance

ABSTRACT

Zn-doped $\text{Li}_3\text{V}_2(\text{PO}_4)_3/\text{C}$ ($\text{Li}_3\text{V}_{2-x}\text{Zn}_x(\text{PO}_4)_3/\text{C}$, $x = 0, 0.02, 0.04$ and 0.06) cathode materials are synthesized by an improved sol–gel method of which pH value is controlled at 4. They are characterized by X-ray diffraction, scanning electron microscopy, high resolution transmission electron microscopy, linear sweep voltammetry, galvanostatic charge/discharge test, cyclic voltammetry, electrochemical impedance spectroscopy and potential step chronoamperometry. $\text{Li}_3\text{V}_{1.96}\text{Zn}_{0.04}(\text{PO}_4)_3/\text{C}$ has the highest electrical conductivity among the four samples. Although the initial discharge capacity for the doped samples at low current rate, such as 0.2C, presents no obvious enhancement compared with that for the undoped one, the cyclability and the rate performance are improved significantly. Zn-doped samples exhibit higher initial discharge capacity than the undoped one as increasing current rates. Among the three Zn-doped samples, $\text{Li}_3\text{V}_{1.96}\text{Zn}_{0.04}(\text{PO}_4)_3/\text{C}$ shows the highest initial discharge capacity of 105.5 mAh g^{-1} at 5C. Capacity retention for $\text{Li}_3\text{V}_{1.96}\text{Zn}_{0.04}(\text{PO}_4)_3/\text{C}$ remains 83.6% at 0.2C after 50 cycles, higher than 62.8% for $\text{Li}_3\text{V}_2(\text{PO}_4)_3/\text{C}$. It is believed that Zn substitution is beneficial to the rate performance and cyclic performance due to the lower charge transfer resistance and higher diffusion coefficient of lithium ions resulted from relatively higher intrinsic conductivity and smaller particle size.

© 2014 Elsevier B.V. All rights reserved.

1. Introduction

Nowadays, lithium ion batteries are extensively used because of its high energy density, excellent charge/discharge capability and good safety [1]. In comparison with layered transition metal oxides LiMO_2 ($M = \text{Co}, \text{Ni}, \text{Mn}$), lithium transition metal phosphates $\text{Li}_x\text{M}_y(\text{PO}_4)_z$ ($M = \text{Fe}, \text{V}$) with strong P–O bonds and three-dimension solid framework can guarantee both dynamic and thermal stability to meet the need of safety performance in electric vehicles (EVs)

and hybrid electric vehicles (HEVs) [2]. In the family of lithium transition metal phosphates, monoclinic $\text{Li}_3\text{V}_2(\text{PO}_4)_3$ has attracted wide attention for its high theoretical capacity (197 mAh g^{-1}) in the instance that all the three Li^+ ions can be reversibly extracted from and reinserted into the host in the voltage range from 3.0 V to 4.8 V. Moreover, its unique NASICON structure provides a 3D framework and a large interstitial space for lithium ions transfer [3]. It is commonly believed that $\text{Li}_3\text{V}_2(\text{PO}_4)_3$ is a promising cathode material due to its high theoretical capacity (197 mAh g^{-1}), good lithium ions diffusion coefficient and suitable operating voltage (3.0–4.8 V) [4–6].

Although it possesses so many advantages, $\text{Li}_3\text{V}_2(\text{PO}_4)_3$ still has some drawbacks, such as low electrical conductivity ($\sim 10^{-7} \text{ S cm}^{-1}$)

^{*} Corresponding author. Tel.: +86 22 27404262; fax: +86 22 27404724.
E-mail address: rsquo@tju.edu.cn (R. Guo).

[7] and poor cycling performance [8,9], thus hindering further practical implementation. There are several significant efforts have been made to overcome these drawbacks, including doping with metal ions [10–13], coating with carbon [9,14] or high electrical conductivity metal oxides [15,16], reducing particle size [5,17] and controlling morphologies of particles [18,19]. It is more preferable to dope $\text{Li}_3\text{V}_2(\text{PO}_4)_3$ with trace elements to improve its intrinsic conductivity. On one hand, V-site substitutions of $\text{Li}_3\text{V}_2(\text{PO}_4)_3$ by Mg^{2+} [20], Cr^{3+} [21], Fe^{2+} [12], Ce^{3+} [22], Nb^{5+} [23] and Ti^{4+} - Mg^{2+} codoping [24] have been extensively explored. Huang et al. [25] considered that in V-site, the existence of Mg^{2+} in $\text{Li}_3\text{V}_2(\text{PO}_4)_3$ compound would cause some local defects in the crystal structure, leading to an increase in electrical conductivity. $\text{Li}_3\text{V}_{1.8}\text{Mg}_{0.03}(\text{PO}_4)_3/\text{C}$ exhibited a good cycle performance, with a retention rate of discharge capacity being 91.4% at 1C after 100 cycles. On the other hand, Chen et al. [26] synthesized $\text{Li}_{3-x}\text{Na}_x\text{V}_2(\text{PO}_4)_3$ ($x = 0, 0.03, 0.05$ and 0.07), in which Li^+ was substituted by Na^+ through a sol–gel method. The $\text{Li}_{2.95}\text{Na}_{0.05}\text{V}_2(\text{PO}_4)_3$ showed a good rate performance. It also delivered an initial capacity of 187 mAh g^{-1} at 0.2C. Ouyang et al. [27] have reported that the band gap of Na-doped LiFePO_4 is much narrower than pure LiFePO_4 materials and energy barrier for Li^+ ions diffusion is decreased after Na doping. Based on this, Kuang et al. [2] suggested that energy barrier for Li^+ ions diffusion in Na-doped $\text{Li}_3\text{V}_2(\text{PO}_4)_3$ was also decreased when compared with those in pure $\text{Li}_3\text{V}_2(\text{PO}_4)_3$. Apart from what mentioned above, PO_4^{3-} substituted by Cl^- has been investigated as well by Yan et al. [28]. In their work, $\text{Li}_3\text{V}_2(\text{PO}_4)_{2.88}\text{Cl}_{0.12}/\text{C}$ composite possessed an excellent discharge capacity as high as 106.9 mAh g^{-1} after 80 cycles at 8C.

Zn doping has been adopted to improve electrochemical performance of LiFePO_4 by Liu et al. [29]. They reported the initial specific discharge capacity of $\text{LiZn}_{0.01}\text{Fe}_{0.99}\text{PO}_4$ was improved by 50.0% at 0.1C compared with that of pure LiFePO_4 . Arumugam et al. [30] synthesized spinel $\text{LiZn}_x\text{Mn}_{2-x}\text{O}_4$ ($x = 0\text{--}0.15$) by sol–gel technique. They found that $\text{LiZn}_{0.1}\text{Mn}_{1.9}\text{O}_4$ exhibited good capacity retention of 87% at a current rate of 0.5C after 100 cycles.

It has been noted that pH value has an obvious influence on the morphologies, particle size and agglomeration of the prepared powders. Dokko et al. [31] prepared LiFePO_4 with needle-like, plate like and randomly shaped morphologies by changing pH value using hydrothermal method. The plate-like crystals exhibited the highest electrochemical reactivity with a discharge capacity being 163 mAh g^{-1} at 0.1C.

An improved sol–gel process has been developed to prepare $\text{Li}_3\text{V}_2(\text{PO}_4)_3/\text{C}$ cathode material and to investigate the influences of different pH values on crystalline structure, morphology, particle size and electrochemical properties of $\text{Li}_3\text{V}_2(\text{PO}_4)_3/\text{C}$ in a previous work of our group [32]. Compared with $\text{Li}_3\text{V}_2(\text{PO}_4)_3/\text{C}$ prepared at pH 7, $\text{Li}_3\text{V}_2(\text{PO}_4)_3/\text{C}$ prepared at pH 4 had relatively better cycle performance and higher initial charge–discharge capacity at low rates. However, the improvements of the initial charge–discharge capacity were limited at high rates, such as 5C. It seems sole changing pH value during the sol–gel process is not sufficient to realize a significant enhancement of comprehensive electrochemical performance. Based on this and considering Zn doping done by Liu et al. [29] and Arumugam et al. [30], we propose that Zn doping may also be helpful to improving electrochemical performance of $\text{Li}_3\text{V}_2(\text{PO}_4)_3/\text{C}$. First, Zn doping can reduce the particle size and make the specific surface area larger, which are beneficial for the electrolyte penetration and lithium ions diffusion. Second, the radius of Zn^{2+} (0.074 nm) is larger than V^{3+} (0.064 nm) in the VO_6 octahedra, so the replacement of vanadium by zinc in the monoclinic structure can cause an increase in the unit cell volume and leads to a distortion of V positions, thus resulting in narrowing band gap of Zn-doped $\text{Li}_3\text{V}_2(\text{PO}_4)_3$ and making lithium ions

diffusion easier. This means the intrinsic conductivity of Zn-doped $\text{Li}_3\text{V}_2(\text{PO}_4)_3$ can be increased. Last, V^{3+} can be oxidized to V^{4+} and V^{5+} during lithium ions extraction–insertion with extraction–expansion of the crystalline lattice, while Zn^{2+} does not participate in the reaction. Thus, Zn doping can play a role in stabilizing the crystalline lattice. It is expected that good crystallinity, small particle size and little agglomeration could be achieved by means of comprehensive effects of both changing pH value and Zn doping. To the best of our knowledge, there are no reports available right now on this aspect.

In this work, Zn-doped $\text{Li}_3\text{V}_2(\text{PO}_4)_3/\text{C}$ ($\text{Li}_3\text{V}_{2-x}\text{Zn}_x(\text{PO}_4)_3/\text{C}$, $x = 0, 0.02, 0.04$ and 0.06) cathode materials were prepared via an improved sol–gel method whose pH value was adjusted to 4. And effects of dopant content on phase composition, microstructure and electrochemical performance of $\text{Li}_3\text{V}_{2-x}\text{Zn}_x(\text{PO}_4)_3/\text{C}$ were investigated.

2. Experimental

$\text{Li}_3\text{V}_{2-x}\text{Zn}_x(\text{PO}_4)_3/\text{C}$ ($x = 0, 0.02, 0.04$ and 0.06 , abbreviated as $\text{Zn}_0, \text{Zn}_2, \text{Zn}_4$ and Zn_6 , respectively) cathode materials were prepared by a sol–gel method in which pH value was controlled at 4 [32]. V_2O_5 (AR, 99.0 wt%, Chemical Reagent Factory of Hunan Coal Science Research Institute, China), ZnO (AR, 99.0 wt%, Kewei Corporation of Tianjin, China), citric acid (AR, 99.5 wt%, Kewei Corporation of Tianjin, China), $\text{NH}_4\text{H}_2\text{PO}_4$ (AR, 99.0 wt%, Kewei Corporation of Tianjin, China) and Li_2CO_3 (AR, 99.0 wt%, Tianjin Benchmark Chemical Reagent Limited Company, China) with a molar ratio of $2\text{--}x\text{:}x\text{:}4\text{:}6\text{:}3$ ($x = 0, 0.02, 0.04, 0.06$) were employed as the starting materials. Citric acid was added simultaneously as chelating reagent, carbon source and reductive agent. First, stoichiometric citric acid, Li_2CO_3 , ZnO and $\text{NH}_4\text{H}_2\text{PO}_4$ were dissolved into 20 mL deionized water, respectively. The citric acid solution was poured into a beaker with V_2O_5 powder inside. Next the mixture was heated to 60°C under continuous stirring until the solution turned to dark blue. Then the Li_2CO_3 , ZnO and $\text{NH}_4\text{H}_2\text{PO}_4$ solutions were added to the dark blue solution. The resultant mixture was heated and maintained at 60°C under continuous stirring for 30 min pH value of the solution was adjusted to be 4 by adding appropriate amount of acetic acid (AR, 36–37 wt%, Tianjin Standard Science and Technology Limited Company, China). The temperature of the mixture was kept at 60°C under continuous stirring for 1 h. Excess water was evaporated at 80°C under continuous stirring until a blue wet gel was obtained. After drying the gel at 80°C for 24 h in an oven, the dry gel was carefully grinded using a mortar and pestle for 1 h. The powders were calcined at 350°C for 5 h in an atmosphere of $95\% \text{ N}_2 + 5\% \text{ H}_2$ in a quartz tube furnace to release H_2O , CO_2 and NH_3 and then further fired at 750°C for 8 h under the same atmosphere. After grinding with the mortar and pestle, the resulted powders were sieved through a 280 mesh screen.

The crystalline phase determination of powders was carried out by an X-ray diffractometer (XRD) with $\text{Cu K}\alpha$ radiation source (D/Max-2500, Rigaku). A step scan mode was adopted with a scan rate of 6° min^{-1} in the 2θ range of $10\text{--}60^\circ$. The morphology of the particles was observed using a scanning electron microscope (SEM, TDCL4800). The morphology and the surface texture of the carbon coated powders were characterized by a high-resolution transmission electron microscope (HRTEM) (Philips, Tecnai G2 F20). The specific surface area measurements were performed on automated surface area analyzer (Quantachrome BET Nova 2000). The content of carbon in different composites was measured by elemental analyzer (Elementar, Vario Micro cube).

The powders were pressed to obtain disk-shaped pellets at 10 MPa for electrical conductivity measurement, using a stainless

steel mould with 12 mm in diameter. The thickness of the pellets is measured by a vernier caliper (usually around 1.5 mm). Then the pellets were fixed in a self-made mould made of an organic insulator. The two sides of the pellets were connected to a Chenhua CHI660C Electrochemical Workstation. Electrical conductivity measurement of powders was adopted with linear sweep voltammetry by a three-probe method and a voltage–current curve was gained. Then the value of the electrical conductivity was calculated by the following equation:

$$\kappa = 4l / \pi R d^2 \quad (1)$$

where κ is the electrical conductivity, R is the resistance obtained from the slope of the linearly fitted line of the voltage–current curve, l is the thickness and d is the diameter.

Electrochemical measurements were performed between 3.0 V and 4.8 V vs. Li^+/Li with coin cells (Type 2430). The cathode film was fabricated by mixing the active material, acetylene black and polyfluorotetraethylene (PTFE) at a weight ratio of 80:15:5 in pure ethanol to form a paste. After rolling to a thin film of 140 μm in thickness, it was cut into circular discs with a diameter of 12 mm. The as-prepared cathode films were assembled into lithium batteries in an argon filled glove box, with Celgard 2400 as a separator, Li foil as counter and reference electrodes. The electrolyte was 1 M LiPF_6 in a mixture of ethylene carbonate (EC) and dimethyl carbonate (DEC) with a volume ratio of 1:1. All the cells were allowed to age for 24 h before testing. The galvanostatic charge/discharge tests were conducted on a Neware battery test system at room temperature. The cyclic voltammetry (CV) tests were conducted at a scanning rate of 0.1 mV s^{-1} within a voltage range of 3.0–4.8 V. In the electrochemical impedance spectroscopy (EIS) tests, the frequency range was from 0.1 Hz to 100 kHz with the amplitude of 5 mV. For the measurements of potential step chronoamperometry (PSCA), an overpotential of 100 mV was applied with response time of 200 s. All the electrochemical measurements were carried out using a Chenhua CHI660C Electrochemical Workstation.

3. Results and discussion

3.1. Sample characterizations

The XRD patterns of Zn_0 , Zn_2 , Zn_4 and Zn_6 powders are shown in Fig. 1. The standard diffraction pattern of $\text{Li}_3\text{V}_2(\text{PO}_4)_3$ is also given for comparison. The XRD patterns of the Zn doped samples are

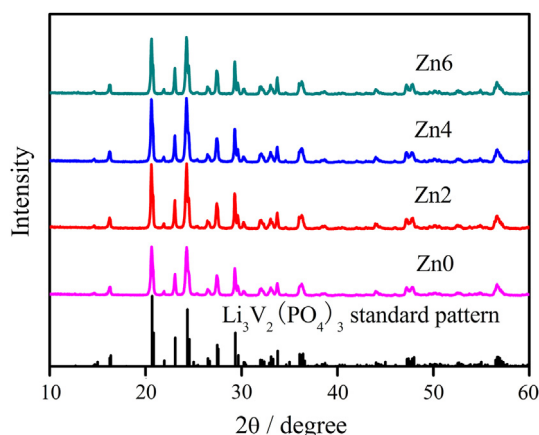


Fig. 1. XRD patterns of Zn_0 , Zn_2 , Zn_4 and Zn_6 powders. The standard XRD pattern of $\text{Li}_3\text{V}_2(\text{PO}_4)_3$ (ICSD # 96962, PDF # 01-072-7074) is also included.

similar to that of the undoped one. No impurity phases are detectable under the resolution of our X-ray diffractometer. This indicates that Zn enters into the crystalline structure of $\text{Li}_3\text{V}_2(\text{PO}_4)_3$. All the diffraction peaks of the as-synthesized powder can be indexed as monoclinic $\text{Li}_3\text{V}_2(\text{PO}_4)_3$ phase (Space group P1 21/n 1, ICSD # 96962, PDF # 01-072-7074). There is no evidence in the XRD patterns for the presence of carbon due to its amorphous state in the composite [28]. The unit cell lattice parameters of all the samples have been refined and the results are summarized in Table 1. The replacement of vanadium by zinc in the monoclinic structure causes an increase in the unit cell volume, which is consistent with the fact that the radius of Zn^{2+} (0.074 nm) is larger than V^{3+} (0.064 nm) in the VO_6 octahedra. The difference of ionic radius between Zn^{2+} and V^{3+} is 13.5%, smaller than 15%, which is calculated by $\Delta = (R_1 - R_2)/R_2$, where R_1 is the radius of the bigger ion (Zn^{2+}) and R_2 is that of the smaller one (V^{3+}). However, the valence of the both ions is different. Therefore, the vanadium can be partially replaced by zinc according to the formation condition of a solid solution [33]. The cell parameters also agree well with those given in several previous reports [22,24,25]. The sole difference lies in the different doping elements and synthesis methods as well.

SEM images of Zn_0 , Zn_2 , Zn_4 and Zn_6 powders are shown in Fig. 2. All the powders are slightly agglomerated. The grain boundary of all the powders is indistinct because of the formed electronic conducting carbon network, leading to a good electron transport among $\text{Li}_3\text{V}_{2-x}\text{Zn}_x(\text{PO}_4)_3/\text{C}$ particles. The Zn_0 powder (Fig. 2(a)) is composed of irregular particles with a broad particle size distribution. The particles of Zn_0 powder aggregate to form mesoporous clusters and networks. However, the particle size of the Zn-doped samples is varied with Zn amount. Appropriate Zn doping content can reduce particle size as well as narrow particle size distribution. Obviously, Zn_4 powder has the smallest particle size and the most uniform morphology (Fig. 2(c)). The reduction of particle size can shorten the diffusion path of lithium ions as well as increase the area for electrode reaction, which is beneficial to improving electrochemical performance as proved later.

In order to prove the existence of carbon layer on the surface of $\text{Li}_3\text{V}_{2-x}\text{Zn}_x(\text{PO}_4)_3/\text{C}$ particles, HRTEM observation of Zn_4 is carried out. As shown in Fig. 3, a thin carbon layer of about 3–4 nm in thickness is coated on surface of the host particle.

Particle size information of Zn_0 , Zn_2 , Zn_4 and Zn_6 powders determined by a laser particle size analyzer is listed in Table 2. It is seen that the particle size analysis results are over all consistent with SEM images as shown in Fig. 2. Zn_4 has the smallest particle size while Zn_6 has the largest one.

Electrical conductivity of Zn_0 , Zn_2 , Zn_4 and Zn_6 powders are shown in Table 3. The conductivity of the undoped powder agrees well with that reported in a previous work [2]. It is obvious that Zn_4 has the highest electrical conductivity among all four samples. Moreover, the electrical conductivity of all the three Zn-doped samples is about one order of magnitude higher compared to that of the undoped one due to the larger radius of Zn^{2+} ion than V^{3+} ion and the different valence state between Zn and V ions. In Zn doped samples, on one hand, the doping of Zn^{2+} ions enlarges crystalline lattices of $\text{Li}_3\text{V}_2(\text{PO}_4)_3$ and leads to a distortion of V positions, thus resulting in narrowing band gap of Zn-doped $\text{Li}_3\text{V}_2(\text{PO}_4)_3$, similar to

Table 1
Refined unit cell lattice parameters for Zn_0 , Zn_2 , Zn_4 and Zn_6 powders.

Sample	<i>a</i> (nm)	<i>b</i> (nm)	<i>c</i> (nm)	β (°)	<i>V</i> (nm ³)
Zn_0	0.8599(3)	1.2055(8)	0.8547(2)	89.148(0)	0.8860(1)
Zn_2	0.8524(7)	1.2085(9)	0.8606(5)	89.509(0)	0.8866(8)
Zn_4	0.8544(7)	1.2051(2)	0.8629(6)	90.439(5)	0.8885(9)
Zn_6	0.8521(7)	1.2095(2)	0.8640(1)	90.284(6)	0.8905(4)

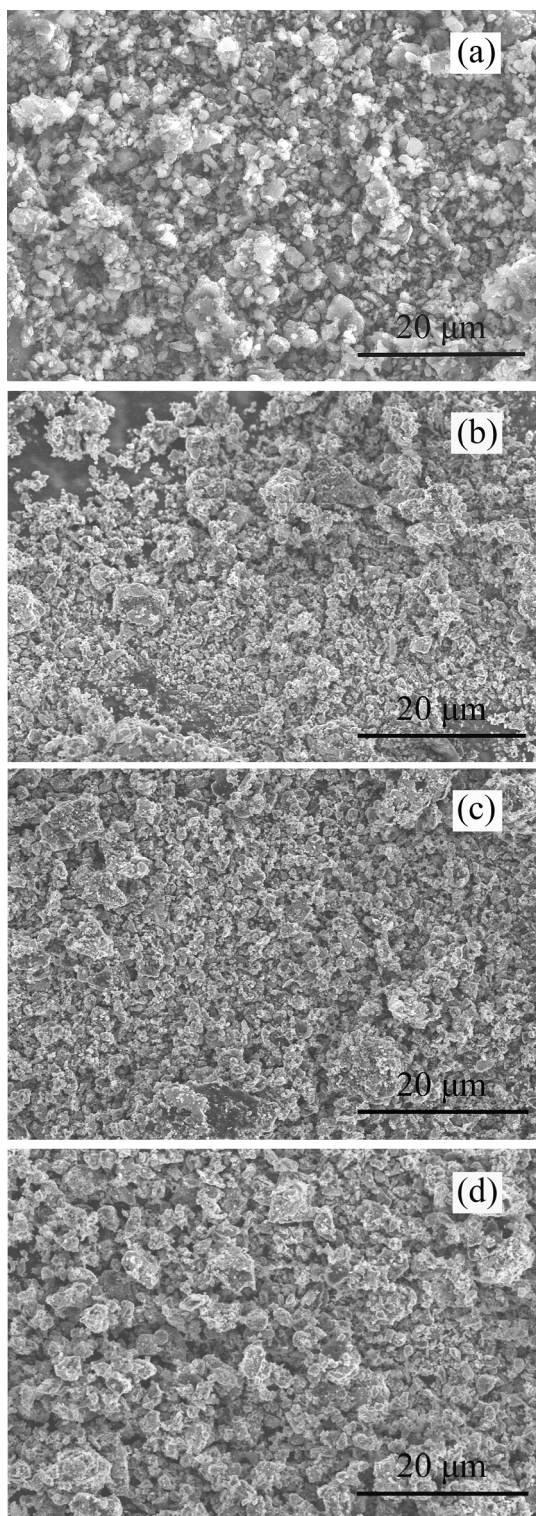


Fig. 2. SEM images of Zn_0 , Zn_2 , Zn_4 and Zn_6 powders with the amplification of 2000 times.

Na -doped $\text{Li}_3\text{V}_2(\text{PO}_4)_3/\text{C}$. Therefore, Zn^{2+} doping can enhance the electrical conductivity of $\text{Li}_3\text{V}_2(\text{PO}_4)_3/\text{C}$ [2]. On the other hand, after Zn^{2+} substitutes onto V^{3+} site, there will generate a hole and V^{4+} in order to preserve charge balance. Consequently, the conductivity increases. This situation has already been reported in Mg -doped $\text{Li}_3\text{V}_2(\text{PO}_4)_3/\text{C}$ [13].

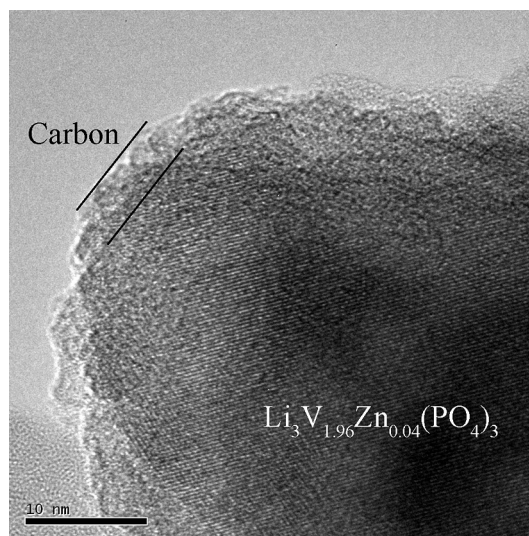


Fig. 3. HRTEM image of Zn_4 showing a carbon layer with 3–4 nm in thickness on the surface of $\text{Li}_3\text{V}_2(\text{PO}_4)_3$ particle.

The content of carbon measured by an elemental analyzer in the samples Zn_0 , Zn_2 , Zn_4 and Zn_6 are also shown in Table 3. It can be easily seen that the content of carbon in doped samples is lower than that of undoped one, in agreement with the case of a previous report [34]. In addition, although the carbon content of Zn_0 is higher than Zn_4 , its electrical conductivity is much lower than that of Zn_4 . Meanwhile, the carbon content between Zn_2 and Zn_4 is relatively close, but the electrochemical performance of Zn_2 is much worse compared with that of Zn_4 . Hence, the enhancement in electrical conductivity is mostly attributed to the Zn doping. It is also believed that the dramatic difference of electrochemical performance among the four samples is not derived from the different contents of carbon.

3.2. Galvanostatic electrochemical performances

Initial charge/discharge curves are shown in Fig. 4 for the four samples in the voltage range of 3.0–4.8 V at room temperature at the current rates of 0.2C, 1C, 2C and 5C, respectively. The two curves of the undoped Zn_0 at 0.2C exhibit four charge voltage plateaus and three discharge voltage plateaus. These plateaus are corresponding to a sequence of transition processes between every two single phases of $\text{Li}_{3-y}\text{V}_2(\text{PO}_4)_3$: $y = 0.0, 0.5, 1.0, 2.0$ and 3.0 [35]. It is noteworthy that the first two charge plateaus were gradually merged into one and became more sloped with an enhancement of current rates. This is caused by the disordering of Li ions during the extraction/reinsertion process [36]. Meanwhile, the potential differences between the charge and discharge plateaus increased and the capacities reduced with increasing current rates, indicating an increased electrical polarization.

The plot shape of Zn -doped samples is basically consistent with that of Zn_0 . However, there are differences, to a certain degree, of charge/discharge behavior among the four cells. It is found discharge capacity of the three Zn -doped samples is not monotonously enhanced with increasing Zn -doping content. It becomes

Table 2
Particle size of Zn_0 , Zn_2 , Zn_4 and Zn_6 powders.

Sample	Zn_0	Zn_2	Zn_4	Zn_6
Particle size (μm)	3.226	2.581	2.248	4.286

Table 3Electrical conductivity and carbon content of Zn₀, Zn₂, Zn₄ and Zn₆ powders.

Sample	Zn ₀	Zn ₂	Zn ₄	Zn ₆
Conductivity (S cm ⁻¹)	8.69×10^{-4}	9.45×10^{-3}	1.14×10^{-2}	8.83×10^{-3}
Carbon content (wt %)	5.73	5.39	5.24	4.85

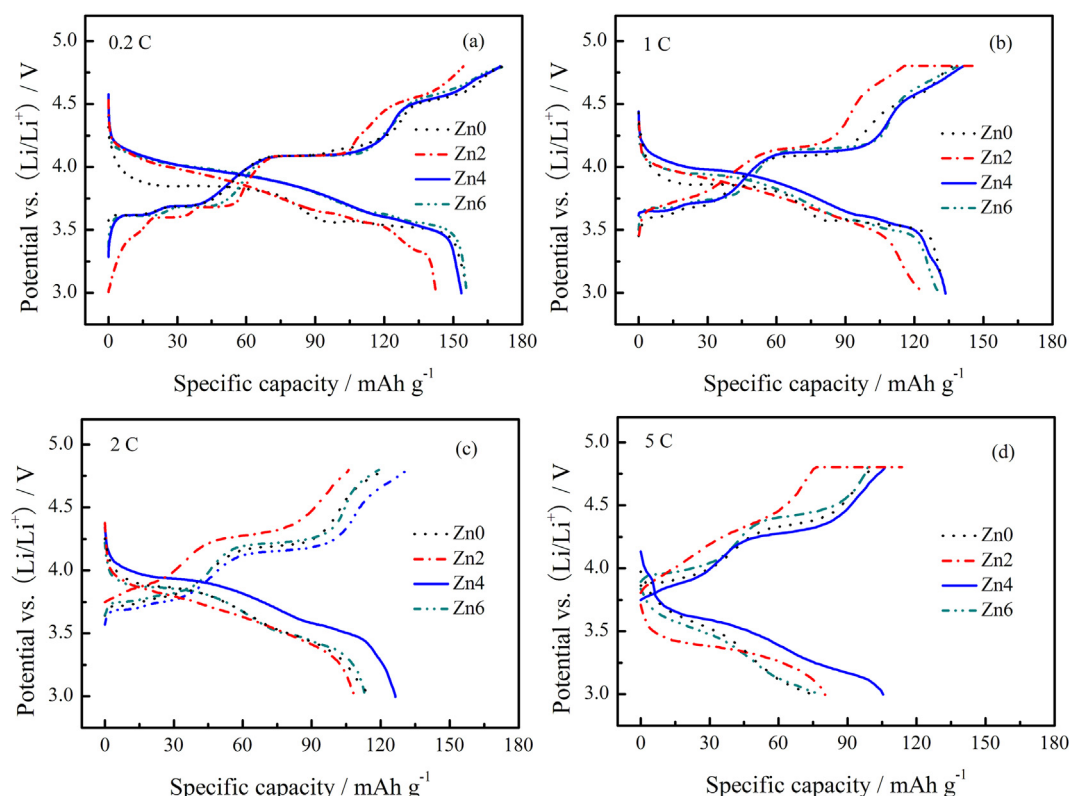
better steadily from Zn₀ to Zn₄ at first and then a decrease is observed at Zn₆. All of these are mainly attributed to Zn overdoping and the differences of electrochemical activities between V³⁺ and Zn²⁺. At low current rate such as 0.2C, although initial discharge capacity for Zn₄ presents no obvious difference compared with that for the undoped one, it is increased at higher rates. The initial discharge capacity of Zn₄ reached 133.4 mAh g⁻¹, 126.4 mAh g⁻¹ and 105.5 mAh g⁻¹ at 1C, 2C and 5C, respectively, while the discharge capacity of Zn₀ are only 131.7 mAh g⁻¹, 115.4 mAh g⁻¹ and 75.2 mAh g⁻¹ at the same rates. It is clear that the improvements of discharge capacity become more significant with increasing current rate after appropriate amount of Zn doping (Zn₄) compared with Zn₀. For instance, the increase of discharge capacity is only 1.7 mAh g⁻¹ (from 131.7 mAh g⁻¹ to 133.4 mAh g⁻¹) at 1C while it is 30.3 mAh g⁻¹ (from 75.2 mAh g⁻¹ to 105.5 mAh g⁻¹) at 5C. All what mentioned above is in a good agreement with the cases of V³⁺ substituted by Fe²⁺ [12], Mg²⁺ [20], Cr³⁺ [21], Ce³⁺ [22] and Nb⁵⁺ [23] in Li₃V₂(PO₄)₃, respectively.

Comparisons of cycle performance and coulombic efficiency of Zn₀, Zn₂, Zn₄ and Zn₆ at 0.2C and 5C is shown in Fig. 5(a) and (b), respectively. As shown in the curves of cycle performance, even though the initial discharge capacity of Zn₀ is higher than that of Zn-doped samples at 0.2C before cycling, the discharge capacity decreases more sharply than that of Zn₂ and Zn₄ after 50 cycles. In

the voltage range of 3.0–4.8 V, the undoped sample shows only capacity retention of 62.8% at 0.2C after 50 cycles, while Zn₂ and Zn₄ remain 67.0% and 83.6% of capacity retention, respectively. It is in keeping with the work of Chung et al. [37]. Chung et al. reported that metal ion doping might allow the formation of more stable phase and enhance the ionic or electronic conductivity, which would improve the specific capacity at high rates and superior cycle-life performance. However, the cycle stability of Zn₆ is severely declined as cycling because of the worse electrochemical activities of Zn²⁺ than V³⁺ as well. It is seen from Fig. 5(b) that Zn₄ still delivers 89.2% of initial discharge capacity (105.5 mAh g⁻¹) after 100 cycles at 5C, much higher than that of the undoped one.

It can also be seen from Fig. 5 that the composites investigated in this work have excellent higher rate performance and superior cycle-life performance comparing with the similar materials at the low rate, for example at 0.2C (50 cycles) and 5C (100 cycles). This case is similar to some previous reports [2,4,13,21,23]. Dong et al. [13] reported that the cycle performance has no much improvement at a low charge/discharge rate (0.1C), while it has an obvious improvement at 5C after Mg doping. The results of Chen et al. [21] exhibited that although there is large decrease in initial specific capacity for all Cr-doped samples at the current rate at 0.2C, both cycle performance and rate capability have been improved markedly when Cr content *x* is no more than 0.1.

The reasons why the composites investigated in this work have excellent higher rate performance and superior cycle-life performance comparing with the similar materials at the low rate are discussed as follows. On one hand, a small content of Zn doping does not influence the structure of the Li₃V₂(PO₄)₃ materials. With increasing the Zn-doping content, the discharge capacity decreases slightly due to the inactive Zn²⁺, similar to Mg doping [13]. Meanwhile, the valence of the zinc and vanadium ions is different. The partial substitution of zinc ions on the interstitial sites requires

**Fig. 4.** Initial charge–discharge curves of Zn₀, Zn₂, Zn₄ and Zn₆ at 0.2C (a), 1C (b), 2C (c) and 5C (d) in the voltage range of 3.0–4.8 V.

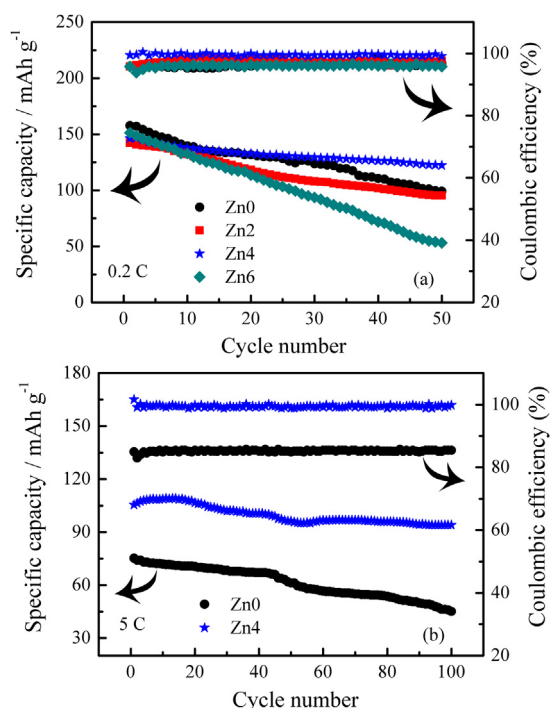


Fig. 5. Cycle performance and coulombic efficiency of all the samples at 0.2C (a) and Zn_0 , Zn_4 at 5C (b).

some associated charge balance to maintain electrical neutrality. This can be accomplished by vacancy formation, substitutional solid solution, or changes in the electronic structure. These defects can result in lattice distortion [33]. However, the defects resulted from Zn doping have a negative effect on the electrochemical performance at low rates. Moreover, the ratio of $\text{V}^{3+}/\text{V}^{4+}$ participating in the reaction decreases after zinc doping. This leads to the decreased electrochemical performance at low rates. On the other hand, the existence of the inactive Zn^{2+} might counteract the volume shrinking/swelling during the Li^+ reversible extraction/insertion, and then increase the cycle stability of $\text{Li}_3\text{V}_2(\text{PO}_4)_3$ system, as Zn^{2+} ions in the Zn doped LiFePO_4 system [29]. For $\text{Li}_3\text{V}_2(\text{PO}_4)_3$ materials, it has been reported that the structural stability of orthorhombic $\text{Li}_3\text{V}_2(\text{PO}_4)_3$ can be enhanced by Nb doping [23]. The authors presented that V^{3+} will be changed to V^{5+} during the lithium de-intercalation process, which could lead to the lattice collapse and limit diffusion of lithium ion. While doping with optimal amount of Nb has a slight effect on the crystal structure of $\text{Li}_3\text{V}_2(\text{PO}_4)_3$ and Nb^{5+} ions may act as a pillar to prevent the collapse of crystal upon cycling. So Nb doping could maintain the structural stability for long-term cycling. It was also reported that metal ion doping might allow the formation of more stable phase and enhance the ionic or electrical conductivity, which would improve the electrochemical properties, including enhanced specific capacity at high rate and superior cycle-life performance [37]. In addition, it is generally accepted that the electrochemical performance is dependent on several factors, including the morphology, particle size and crystallinity [23]. The Zn_4 exactly satisfied the

above conditions, with optimized particle size and shape, so it exhibits the highest discharge capacity and the best capacity retention ratio [38]. And the advantage of smallest particle size is sufficiently reflected at high rates according to the mosaic model proposed for LiFePO_4 cathode materials [32]. Consequently, the rate performances and the cyclic performances of the $\text{Li}_3\text{V}_2(\text{PO}_4)_3$ system were apparently improved through the doping of suitable amount of Zn at the high charge/discharge rates.

The coulombic efficiency given in Table 4 is the average of the coulombic efficiency from the first cycle to the 50th cycle at 0.2C and from the first cycle to the 100th cycle at 5C as shown in Fig. 5. It is obvious that all the samples have a similar coulombic efficiency at low rate such as 0.2C, while the coulombic efficiency of Zn_0 and Zn_4 at the high rate of 5C varies greatly. In addition, the coulombic efficiency of Zn_4 at 5C is close to 100% during the whole cycling, highlighting good electrochemical reversibility [39]. This result can explain the cycle performance to a certain degree.

On the whole, Zn_4 exhibited an optimum initial discharge capacity and cycle performance, especially at 5C. This can be explained by the improved microstructure and higher electrical conductivity. As mentioned above, Zn_4 composite has the smallest particle size and the most uniform morphology. The Li ions only need to diffuse over shorter distance between the surface and center during lithium insertion or extraction within a smaller particle. Smaller particles also have a larger specific surface area for contacting with electrolyte, which can provide more chances for electron conducting. Besides, with the increase of cycle times, there is concentration polarization between the surface and center of the active material, resulting in a decrease of discharge capacity. After Zn-doping, the formation of more stable phase can prohibit the polarization. In addition, as reported in a previous article [32], the active material with a finer particle size can almost fully contribute to the charge–discharge capacity according to the mosaic model proposed for LiFePO_4 cathode materials. So the advantage of small particle size is sufficiently reflected at high rates.

Fig. 6 shows rate performances of Zn_0 and Zn_4 . The discharge capacity of Zn_0 is 46.8 mAh g^{-1} after the 10th cycle at 5C, remaining 30.7%. As a comparison, the capacity is 139.9 mAh g^{-1} after the 10th cycle at 0.1C, with a retention of 91.8%. An intrinsic defect of $\text{Li}_3\text{V}_2(\text{PO}_4)_3$ may take responsibility for this decay behavior [9,23,28]. After Zn-doping, even though the capacity retention has no clear difference after 10 cycles at 0.1C, significant enhancements of capacity retention at elevated rates are clearly observed. A retention of 42.5% is obtained for Zn_4 sample after 10 cycles at 5C. Zn substitution is substantially beneficial to the rate performance because of the higher diffusion coefficient of lithium ions resulted

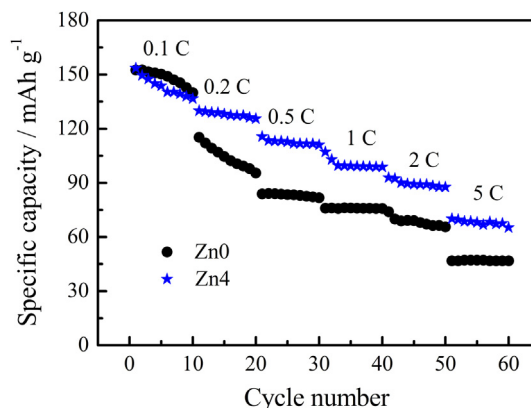


Fig. 6. Rate performance of Zn_0 and Zn_4 in the voltage range of 3.0–4.8 V.

Table 4
Coulombic efficiency of all the prepared samples.

Sample	Zn_0	Zn_2	Zn_4	Zn_6
Coulombic efficiency at 0.2C (%)	96.29	97.46	99.53	95.97
Coulombic efficiency at 5C (%)	85.20	/	99.42	/

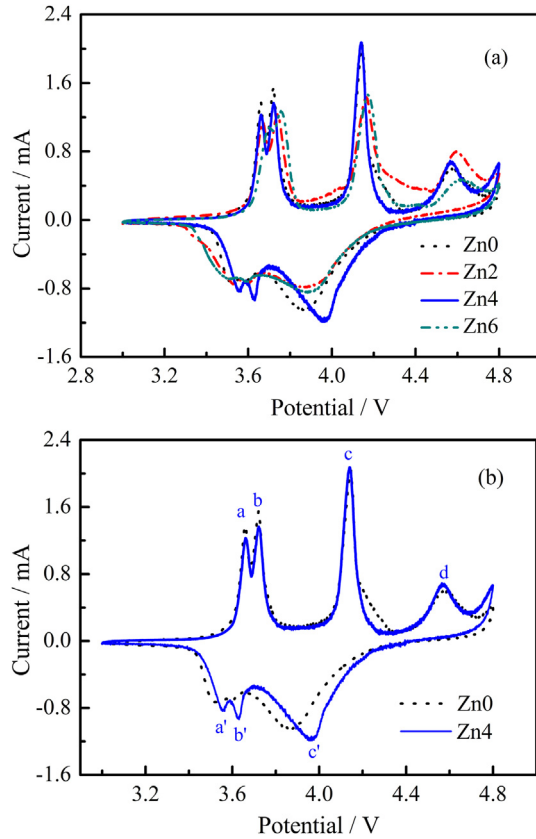


Fig. 7. Cyclic voltammetry profiles of Zn₀, Zn₂, Zn₄ and Zn₆ at a scanning rate of 0.1 mV s⁻¹ in the voltage range of 3.0–4.8 V.

from the relatively higher intrinsic conductivity and the smaller particle size.

3.3. Cyclic voltammetry

CV curves of Zn₀, Zn₂, Zn₄ and Zn₆ between 3.0 and 4.8 V are shown in Fig. 7(a). In order to show more clearly the difference of the plots, CV curves of Zn₀ and Zn₄ are redrawn in Fig. 7(b). It is seen that all the curves show a similar profile. There are four oxidation peaks and three reduction peaks in all the curves, indicating that the reaction behavior does not change during lithium extraction/insertion process. In the differential CV curves, the first two sharp oxidation peaks are associated with the extraction of the first Li ion. As is shown in Fig. 7(b), the four oxidation peaks of the undoped sample are located at around 3.66 V, 3.72 V, 4.15 V and 4.57 V, respectively, and three reduction peaks are located at around 3.52 V, 3.60 V and 3.87 V, respectively. However, some significant changes can be observed in the Zn-doped samples. Taking Zn₄ electrode as an example, the reduction peaks shift up to 3.54 V, 3.61 V and 3.90 V, respectively. Table 5 gives potential differences between oxidation and reduction peaks for all the samples. It is

Table 5
Potential differences between the oxidation and reduction peaks for Zn₀, Zn₂, Zn₄ and Zn₆.

Sample	$\Delta E_{a-a'}$ (V)	$\Delta E_{b-b'}$ (V)	$\Delta E_{c-c'}$ (V)	$\Delta E_{d-d'}$ (V)
Zn ₀	0.141	0.122	0.279	0.710
Zn ₂	0.142	0.140	0.282	0.715
Zn ₄	0.120	0.113	0.239	0.664
Zn ₆	0.144	0.178	0.288	0.743

clear the potential differences are the smallest for Zn₄ electrode. The well-defined peaks and smaller value of potential interval are the reasons for the enhancement of electrode reaction reversibility.

Meanwhile, Zn₄ has the highest peak of current density among all the four samples. As is known, the relationship between current density and diffusion coefficient of lithium ions is complied with the following Eq. (2) [30]:

$$i_p = 2.69 \times 10^5 n^{3/2} A C_0 D^{1/2} \nu^{1/2} \quad (2)$$

where i_p is the peak current, n is the number of electrons transferred per molecule during the intercalation, A is the contact area between active material and electrolyte, C_0 is the concentration of lithium ions, D is the diffusion coefficient of lithium ions, and ν is the scan rate. Since i_p is proportional to $D^{1/2}$, it is rationally deduced that the Li⁺ ion diffusion coefficient of Zn₄ is also the highest [31]. This is ascribed to the small particle size, slight agglomeration and good crystallization.

3.4. EIS and PSCA analyses

Electrochemical impedance spectroscopy (EIS) measurements were carried out to study the effect of Zn doping on the impedance response. EIS tests were performed on all the samples at the fully discharged state. Fig. 8(a) shows the Nyquist plots of Zn₀, Zn₂, Zn₄ and Zn₆. All the impedance spectra are composed of a depressed semicircle in the moderate frequency region and a straight sloping line in the low frequency region. The semicircle is related to the charge transfer process. The numerical value of the diameter of the semicircle on the Z' axis is approximated as the charge transfer resistance (R_{ct}). The straight beeline is attributed to the Warburg

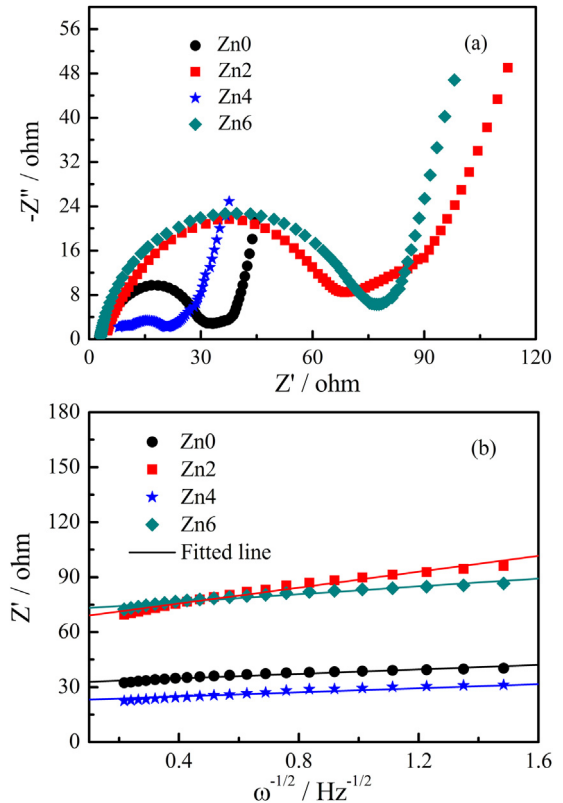


Fig. 8. EIS spectra of all the samples in the frequency range between 0.1 Hz and 100 kHz with the amplitude of 5 mV (a) and the relationship between Z' and square root of frequency ($\omega^{-1/2}$) in the low-frequency region (b).

Table 6
Kinetic parameters of Zn₀, Zn₂, Zn₄ and Zn₆.

Sample	R_{ct} (Ω)	σ	b	K	D_{Li^+} ($\text{cm}^2 \text{s}^{-1}$)/EIS	D_{Li^+} ($\text{cm}^2 \text{s}^{-1}$)/PSCA	D_{Li^+} ($\text{cm}^2 \text{s}^{-1}$)/CV
Zn ₀	32.72	6.13	12.610	31.456	5.40×10^{-11}	5.33×10^{-9}	6.82×10^{-9}
Zn ₂	71.18	21.68	12.152	23.870	4.32×10^{-12}	5.50×10^{-9}	3.38×10^{-9}
Zn ₄	20.39	5.59	17.869	23.857	6.50×10^{-11}	9.03×10^{-9}	7.42×10^{-9}
Zn ₆	79.77	10.69	7.966	33.727	1.78×10^{-11}	3.26×10^{-9}	3.70×10^{-9}

impedance, which is associated with the diffusion of Li⁺ ions in the electrode [24,25]. It can be easily inferred through comparing the semicircles of all the samples shown in Fig. 8(a) that Zn₄ has the smallest charge transfer resistance (R_{ct}) among the four samples.

In order to understand influences of Zn doping on the diffusion coefficient of Li⁺ ion (D), the EIS result is fitted (Fig. 8(b)). The diffusion coefficient of Li⁺ ion (D) are calculated according to the following Eq. (3):

$$D = R^2 T^2 / 2A^2 n^4 F^4 C^2 \sigma^2 \quad (3)$$

where R is the gas constant, T is the absolute temperature, A is the surface area of the cathode, n is the number of electrons per molecule during oxidation, F is the Faraday constant, C is the concentration of lithium ion, and σ is the Warburg factor which has a relationship with Z' as follows [29,40]:

$$Z' = R_e + R_{ct} + \sigma \omega^{-1/2} \quad (4)$$

where R_e is the resistance between the electrolyte and electrode, R_{ct} is the charge transfer resistance, and ω is angle frequency. Fig. 8(b)

shows the relationship between Z' and square root of frequency ($\omega^{-1/2}$) in the low-frequency region. A linear characteristic is seen for all the curves. σ , the slope of the linearly fitted lines of Z' vs. $\omega^{-1/2}$, is listed in Table 6. The value of Warburg factor is 6.13, 21.68, 5.59 and 10.69 corresponding to Zn₀, Zn₂, Zn₄ and Zn₆, respectively. Since D is proportional to σ^{-2} , it is easily concluded that the sample of Zn₄ has the highest lithium ion diffusion coefficient.

To further understand the reason for an improved electrochemical performance of Zn-doped samples, the potential step chronoamperometry (PSCA) measurement was performed after fully discharged to 3.0 V Fig. 9(a) shows the chronoamperometry $I-t$ curves. Fig. 9(b) is the $I-t^{1/2}$ curve which is converted from Fig. 9(a). D_{Li^+} can be obtained from the following equation:

$$D_{Li^+} = \frac{b^2 R^2}{\pi K^2} \quad (5)$$

where, b is the intercept, K is the slope of the fitted line, and R is the average radius of each powder [41]. All the parameters obtained from the PSCA are given in Table 6. It can be observed that the D_{Li^+} is $9.03 \times 10^{-9} \text{ cm}^2 \text{s}^{-1}$ for the sample of Zn₄. This value is the highest among all the four samples, in agreement with the rate capability and EIS results.

Moreover, the diffusion coefficient of lithium ion determined from different methods is also summarized in Table 6. It is found that although the diffusion coefficients are slightly different and ranges from 10^{-9} to $10^{-12} \text{ cm}^2 \text{s}^{-1}$, they are very close to the values reported by Chen et al. [26]. In addition, Zn₄ has always the fastest lithium ion diffusion regardless which method is used. This is consistent with the above electrochemical results.

4. Conclusions

Zn₀, Zn₂, Zn₄ and Zn₆ were successfully synthesized by an improved sol-gel process in which pH value was controlled at 4. Galvanostatic electrochemical measurements indicated that Zn₄ exhibited the best electrochemical performances in the voltage range of 3.0–4.8 V, especially at high rates. Zn₄ shows the highest initial discharge capacity of 105.5 mAh g^{-1} at 5C, while the discharge capacity of the undoped sample is only 75.2 mAh g^{-1} . After 100 cycles, capacity retention for Zn₄ remains 89.2%, much higher than 60.0% for Zn₀. The lower charge transfer resistance and higher diffusion coefficient of lithium ions are responsible for the outstanding electrochemical performance of the Zn-doped composites, which resulted from the small particle size, slight agglomeration, good crystallization and high intrinsic conductivity.

Acknowledgments

This work was supported by the National Natural Science Foundation of China under grant No. 51372165. Professor Guangchuan Liang (School of Materials Science and Engineering, Hebei University of Technology, China) is gratefully appreciated for his helps.

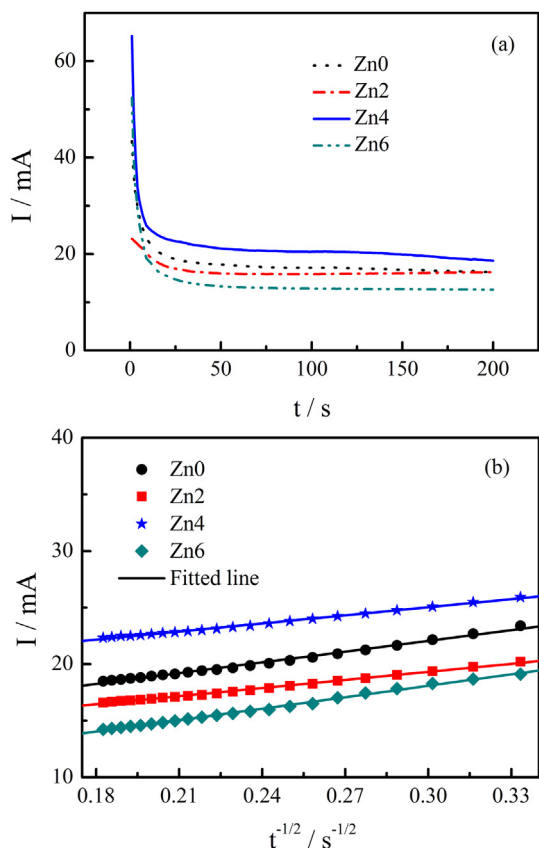


Fig. 9. PSCA curves of all the samples with a potential step of 100 mV in 200 s (a) and the relationship between I and $t^{-1/2}$ (b).

References

- [1] Z. Liu, F. Huang, J. Sun, *Mater. Sci. Eng. B* 176 (2011) 1313.
- [2] Q. Kuang, Y. Zhao, Z. Liang, *J. Power Sources* 196 (2011) 10169.
- [3] W. Yuan, J. Yan, Z. Tang, O. Sha, J. Wang, W. Mao, L. Ma, *J. Power Sources* 201 (2012) 301.
- [4] F. Teng, Z.-H. Hu, X.-H. Ma, L.-C. Zhang, C.-X. Ding, Y. Yu, C.-H. Chen, *Electrochim. Acta* 91 (2013) 43.
- [5] Y.N. Ko, J.H. Kim, Y.J. Hong, Y.C. Kang, *Mater. Chem. Phys.* 131 (2011) 292.
- [6] X. Zhang, H. Guo, X. Li, Z. Wang, L. Wu, *Solid State Ionics* 212 (2012) 106.
- [7] Y.Q. Qiao, J.P. Tu, X.L. Wang, C.D. Gu, *J. Power Sources* 199 (2012) 287.
- [8] J. Yan, W.-F. Mao, H. Xie, Z.-Y. Tang, W. Yuan, X.-C. Chen, Q. Xu, L. Ma, *Mater. Res. Bull.* 47 (2012) 1609.
- [9] X.H. Rui, C. Li, C.H. Chen, *Electrochim. Acta* 54 (2009) 3374.
- [10] W. Yuan, J. Yan, Z. Tang, O. Sha, J. Wang, W. Mao, L. Ma, *Electrochim. Acta* 72 (2012) 138.
- [11] D. Ai, K. Liu, Z. Lu, M. Zou, D. Zeng, J. Ma, *Electrochim. Acta* 56 (2011) 2823.
- [12] M. Ren, Z. Zhou, Y. Li, X.P. Gao, J. Yan, *J. Power Sources* 162 (2006) 1357.
- [13] Y.Z. Dong, Y.M. Zhao, H. Duan, *J. Electroanal. Chem.* 660 (2011) 14.
- [14] Y. Li, L. Hong, J. Sun, F. Wu, S. Chen, *Electrochim. Acta* 85 (2012) 110.
- [15] L.-L. Zhang, G. Liang, G. Peng, F. Zou, Y.-H. Huang, M.C. Croft, A. Ignatov, *J. Phys. Chem. C* 116 (2012) 12401.
- [16] J. Zhai, M. Zhao, D. Wang, Y. Qiao, *J. Alloys. Compd.* 502 (2010) 401.
- [17] Y. Li, Z. Zhou, M. Ren, X. Gao, J. Yan, *Electrochim. Acta* 51 (2006) 6498.
- [18] Z. Z. M.M. Ren, X.P. Gao, W.X. Peng, J.P. Wei, *J. Phys. Chem. C* 112 (2008) 5689.
- [19] Y.N. Ko, H.Y. Koo, J.H. Kim, J.H. Yi, Y.C. Kang, J.-H. Lee, *J. Power Sources* 196 (2011) 6682.
- [20] Y.G. Mateyshina, N.F. Uvarov, *J. Power Sources* 196 (2011) 1494.
- [21] Y. Chen, Y. Zhao, X. An, J. Liu, Y. Dong, L. Chen, *Electrochim. Acta* 54 (2009) 5844.
- [22] J. Yao, S. Wei, P. Zhang, C. Shen, K.-F. Aguey-Zinsou, L. Wang, *J. Alloys. Compd.* 532 (2012) 49.
- [23] Y. Xia, W. Zhang, H. Huang, Y. Gan, C. Li, X. Tao, *Mater. Sci. Eng. B* 176 (2011) 633.
- [24] C. Deng, S. Zhang, S.Y. Yang, Y. Gao, B. Wu, L. Ma, B.L. Fu, Q. Wu, F.L. Liu, *J. Phys. Chem. C* 115 (2011) 15048.
- [25] J.S. Huang, L. Yang, K.Y. Liu, Y.F. Tang, *J. Power Sources* 195 (2010) 5013.
- [26] Q. Chen, X. Qiao, Y. Wang, T. Zhang, C. Peng, W. Yin, L. Liu, *J. Power Sources* 201 (2012) 267.
- [27] C.Y. Ouyang, D.Y. Wang, S.Q. Shi, Z.X. Wang, H. Li, X.J. Huang, L.Q. Chen, *Chin. Phys. Lett.* 23 (2006) 61.
- [28] J. Yan, W. Yuan, Z.-Y. Tang, H. Xie, W.-F. Mao, L. Ma, *J. Power Sources* 209 (2012) 251.
- [29] H. Liu, Q. Cao, L.J. Fu, C. Li, Y.P. Wu, H.Q. Wu, *Electrochem. Commun.* 8 (2006) 1553.
- [30] D. Arumugam, G.P. Kalaigan, K. VEDIAPPAN, C.W. Lee, *Electrochim. Acta* 55 (2010) 8439.
- [31] K. Dokko, S. Koizumi, H. Nakano, K. Kanamura, *J. Mater. Chem.* 17 (2007) 4803.
- [32] W.W. Xu, L. Liu, H.L. Guo, R.S. Guo, C. Wang, *Electrochim. Acta* 113 (2013) 497.
- [33] W.D. Kingery, H.K. Bowen, D.R. Uhlmann, *Introduction to Ceramics*, second ed., Wiley-Interscience, New York, 1976, pp. 131–139.
- [34] Y.A. Huang, Y.L. Xu, X. Yang, *Electrochim. Acta* 113 (2013) 156.
- [35] S.-C. Yin, H. Grondy, P. Strobel, M. Anne, L.F. Nazar, *J. Am. Chem. Soc.* 125 (2003) 10402.
- [36] Q. Kuang, Y.M. Zhao, *J. Power Sources* 216 (2012) 33.
- [37] S.Y. Chung, J.T. Bloking, Y.M. Chiang, *Nat. Mater.* 1 (2002) 123.
- [38] L.L. Ge, C.X. Han, L.P. Ni, J. Zhang, Y.L. Tao, Q.B. Yu, Y.H. Shen, A.J. Xie, L. Zhu, Y.P. Zhang, *Solid State Sci.* 14 (2012) 864.
- [39] T. Jiang, W.C. Pan, J. Wang, X.F. Bie, F. Du, Y.J. Wei, C.Z. Wang, G. Chen, *Electrochim. Acta* 55 (2010) 3864.
- [40] X.Y. Du, W. He, X.D. Zhang, Y.Z. Yue, H. Liu, X.G. Zhang, D.D. Min, X.X. Ge, Y. Du, *J. Mater. Chem.* 22 (2012) 5960.
- [41] J.M. Cao, Y. Qu, R.S. Guo, *Electrochim. Acta* 67 (2012) 152.